Three-dimensional scale-dependent Rayleigh-Taylor dynamics with variable acceleration in a finite-size domain: Part II. Solutions of spikes in linear and nonlinear regimes

By H. Hwang AND S. I. Abarzhi†

1. Motivation and objectives

Rayleigh-Taylor instability (RTI) develops large coherent flow structures, bubbles and spikes in the late-time regime and evolves into the mixing regime. Solutions of bubbles for 3D RTI with time-dependent acceleration in the finite-size domain were rigorously derived in Hwang & Abarzhi (2020a,b). In the linear regime, diagnostic parameters such as curvature and velocity grows exponentially. In the nonlinear regime, parameters of the bubbles are derived as a family of asymptotic solutions, assuming the acceleration power-law in time. Applying the consistent approach, the solutions for spike evolution can be derived; however, special attention is required due to fundamentally different characteristics of spikes and bubbles.

Experiments show significantly different dynamics for spikes and bubbles; bubbles move with the same velocity whereas spikes accelerate in the nonlinear regime, the curvature of spikes is more pronounced, and small vortical structures appreciably develop on spikes (Jacobs & Catton 1988; Meshkov 2013). Also, Meshkov & Abarzhi (2019) demonstrate that the mixing zone is dominated by spikes. Due to the distinctive features of spikes, understanding the dynamics of spikes in RTI is crucial. However, spikes are exceptionally challenging to study as prior models show limiting behavior and predictions (Mikaelian 2014).

In this study, the dynamics of spikes in both linear and nonlinear regimes are focused on 3D RTI with time-varying acceleration in the finite domain. We apply the methodology developed in Hwang & Abarzhi (2020a,b). A continuous family of asymptotic solutions is derived in the nonlinear regime. The difference between solutions for spikes and those for bubbles is identified. The convergence limit in terms of Fourier amplitude approximation is detailed. Special solutions are illustrated and the mechanism of the transitions from the scale-dependent dynamics to the self-similar mixing for RT spikes is analyzed.

2. Methodology

The boundary value problem in Hwang & Abarzhi (2020a,b) is revisited, focusing on the solutions of spikes. A simple system of RTI is configured as the heavier fluid is located above the lighter fluid and the unperturbed interface between the two fluids is horizontally parallel. The time-dependent acceleration is in the direction normal to the interface. Our approach applies the group theory to the subspace group p4mm and

† University of Western Australia, Australia.

the truncation of Fourier amplitudes is demonstrated in the aforementioned studies. We exploit the consistent methodology here to describe the dynamics of spikes for 3D RTI.

2.1. *Boundary value problem*

The irreducibility and the symmetry of the flow are determined by the group theory for p4mm and permit the fluid potentials as

$$\Phi_h(x,y,z,t) = \sum_{m,n=1}^{\infty} \Phi_{mn}(t)\,\Big(y\sinh\left(m\alpha_{mn}L\right) + \frac{\cos\left(mkx\right)\cos\left(nkz\right)}{m\alpha_{mn}}\cosh\left[m\alpha_{mn}(y-L)\right]\Big) + f_h(t) + c.c, \tag{2.1a}$$

$$\Phi_l(x,y,z,t) = \sum_{m,n=1}^{\infty} \widetilde{\Phi}_{mn}(t)\,\Big(-y\sinh\left(m\alpha_{mn}L\right) + \frac{\cos\left(mkx\right)\cos\left(nkz\right)}{m\alpha_{mn}}\cosh\left[m\alpha_{mn}(y+L)\right]\Big) + f_l(t) + c.c, \tag{2.1b}$$

in a spatial coordinate system, where $(x_1, x_2, x_3) = (x, y, z)$ such that x and y constitute the horizontal plane, which is vertical to the acceleration, and z represents the vertical space. t denotes time. α_{mn} is defined as $\alpha_{mn}^2 = m^2 + n^2$, with integers $m, n = 1, 2, 3\ldots$. Here, Φ_{mn} is the matrix of Fourier amplitudes, with $\Phi_{mn} = \Phi_{nm}$ and $\Phi_{00} = 0$. $f_h(t)$ and $f_l(t)$ are time-dependent functions and $c.c$ are cross-terms. We note that the velocity $\mathbf{v}_{h,l}$ is related to the fluid potentials as $\mathbf{v}_{h,l} = \nabla\Phi_{h,l}$ and the continuity condition is automatically satisfied as $\Delta\Phi_{h,l} = 0$.

The spatial expansions of interface $z^*(x,y,t)$ with the symmetry constraints only permit

$$z^*(x,y,t) = \sum_{i,j=0}^{\infty} \zeta_{i,j} x^{2i} y^{2j}. \tag{2.2}$$

2.2. *Dynamical system: 3D p4mm*

The identical expressions for moments M, N and truncation in Hwang & Abarzhi (2020a,b) are introduced for the solutions of spikes. Dynamical system with the indenpendent moments are written as

$$\dot{\zeta_1} - 2N_{0,0,1}\zeta_1 - \frac{M_{0,0,2}}{4} = 0, \quad \dot{\zeta_1} - 2\widetilde{N}_{0,0,1}\zeta_1 + \frac{\widetilde{M}_{0,0,2}}{4} = 0$$

$$(1+A)\left(\frac{\dot{N}_{0,0,1}}{4} + \zeta_1\dot{M}_0 - \frac{N_{0,0,1}^2}{8} - g\zeta_1\right) = (1-A)\left(\frac{\dot{\widetilde{N}}_{0,0,1}}{4} - \zeta_1\dot{\widetilde{M}}_0 - \frac{\widetilde{N}_{0,0,1}^2}{8} - g\zeta_1\right)$$

$$M_0 + \widetilde{M}_0 = 0. \tag{2.3}$$

Recall that the choice of Fourier approximation is arbitrary. In the linear regime, only the first harmonic is retained. In the nonlinear regime, we seek the solutions of spikes to the second harmonic of the moments M, N $(\Phi_{10}, \Phi_{20}, \widetilde{\Phi}_{10}, \widetilde{\Phi}_{20})$ as Fourier amplitudes (Abarzhi & Inogamov 1995; Abarzhi 1996). This choice of Fourier approximation leads to a continuous familty of asymptotic solutions.

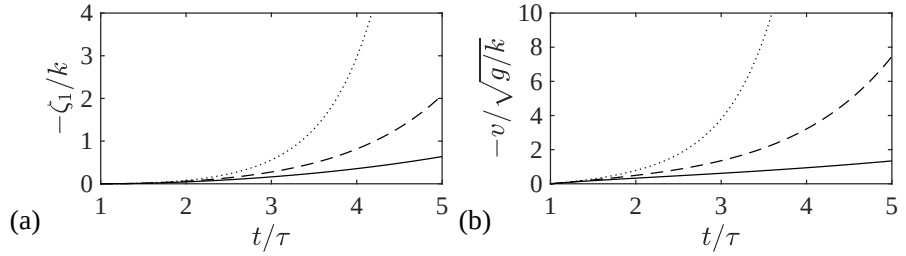

FIGURE 1. Linear regime solutions. (a) The curvature ζ_1 and (b) the velocity v for spikes for the subspace group p4mm. The curvature and the velocity are shown for the Atwood number $A = 0.7$ with two different finite-size domains $kZ = 5$ (black lines) and $kZ = 0.5$ (gray lines). The acceleration exponents are $a = -1$ (solid lines), $a = 0$ (dashed line) and $a = 1$ (dotted line).

3. Results

The dynamical system in Eq. (2.3) is consistently applied to both linear and nonlinear regimes for the Atwood number, $0 < A \leq 1$. In this section, we identify the solutions of RT spikes.

3.1. *Early-time dynamics*

The curvature ζ_1 and the velocity v at the tip of RT spikes with the acceleration exponent $a > -2$ are derived with the assumptions that $(t - t_0) \ll \tau$ with $t \gg \tau$ and $t \gg t_0$, where $\tau = \tau_G$ (e.g., see Hwang & Abarzhi 2020a). The small initial amplitude and velocity assumptions lead to the following solution in the linear regime

$$\xi = C_1 \sqrt{\frac{t}{\tau}} I_{\frac{1}{2s}} \left(\sqrt{A \tanh(kZ)} \frac{(t/\tau)^s}{s} \right) + C_2 \sqrt{\frac{t}{\tau}} I_{-\frac{1}{2s}} \left(\sqrt{A \tanh(kZ)} \frac{(t/\tau)^s}{s} \right) \quad (3.1)$$

$$v = -\frac{4}{k} \frac{\mathrm{d}\xi}{\mathrm{d}t}, \quad (3.2)$$

where $s = (a+2)/2$ and I_p is the modified Bessel function of the pth order. The curvature ζ_1 has a positive value for spikes as it is concave up $\widehat{\overline{\zeta}} > 0$, whereas bubbles have negative curvature and concave down $\widehat{\overline{\zeta}} > 0$ Hwang & Abarzhi (2020a). Also, we note that spikes move downward $\widehat{\overline{v}} < 0$ while bubbles move upward $\overline{v} > 0$ in the current configuration. Thus, the magnitude of solutions for bubbles and spikes in the linear regimes is identical but differs only in sign.

The dimensionless curvature $\xi = \zeta_1/k$ and the velocity $-v/\sqrt{g/k}$ for spikes with the Atwood number $A = 0.7$ are shown in Figure 1. As the acceleration exponent a increases from $a = -1$ to $a = 1$, spikes are more curved and faster. The effects of finite-size domain kZ on v and ξ are illustrated by comparing the black lines ($kZ = 5$) and gray lines ($kZ = 0.5$). v and ξ increase at a slower rate for the larger finite-size domain kZ.

3.2. *Late-time dynamics*

A one-parameter family of asymptotic solutions in the form of power-law function is sought for p4mm RTI ($a > -2$). The readers are referred to Hwang & Abarzhi (2020b) for the detailed derivation of the nonlinear solutions. In order to map the solutions expressed in the finite-size domain to the expressions in the infinite-size domain, fundamental scales in Hwang & Abarzhi (2020a) are applied to describe solutions of spikes in the nonlinear regime. From the dynamical system in Eq. (2.3), the continuous family of the asymptotic

solutions for the velocity v and the shear Γ reads as

$$v_\infty = \mu\frac{\sqrt{2}}{k\tau}\left(\frac{t}{\tau}\right)^{\frac{a}{2}}(A\xi)^{\frac{1}{2}}(3-8\xi)(3+8\xi)\mathcal{D}, \quad \Gamma_\infty = \mu\frac{12\sqrt{2}}{\tau}\left(\frac{t}{\tau}\right)^{\frac{a}{2}}(A\xi)^{\frac{1}{2}}\mathcal{D}, \tag{3.3}$$

where $\mathcal{D}$ is defined as $\mathcal{D} = \left\{48\xi - A(9+64\xi^2)\right\}^{-1/2}$. Also, the subscript ∞ denotes the solutions in the infinite-size domain. μ determines the sign of the velocity and shear as $\mu > 0$ for bubbles and $\mu < 0$ for spikes, thus leading to upward propagating bubbles $v > 0$ and downward propagating spikes $v < 0$ in the present setup. Moreover, the Fourier amplitudes are

$$\Phi_{1\infty} = \frac{-4\sqrt{2}}{k\tau}\left(\frac{t}{\tau}\right)^{\frac{a}{2}}(A\xi)^{\frac{1}{2}}(3-8\xi)(1+4\xi)\mathcal{D}, \tag{3.4a}$$

$$\Phi_{2\infty} = \frac{\sqrt{2}}{k\tau}\left(\frac{t}{\tau}\right)^{\frac{a}{2}}(A\xi)^{\frac{1}{2}}(3-8\xi)(1+8\xi)\mathcal{D}, \tag{3.4b}$$

$$\widetilde{\Phi}_{1\infty} = \frac{4\sqrt{2}}{k\tau}\left(\frac{t}{\tau}\right)^{\frac{a}{2}}(A\xi)^{\frac{1}{2}}(3+8\xi)(1-4\xi)\mathcal{D}, \tag{3.4c}$$

$$\widetilde{\Phi}_{2\infty} = \frac{-\sqrt{2}}{k\tau}\left(\frac{t}{\tau}\right)^{\frac{a}{2}}(A\xi)^{\frac{1}{2}}(3+8\xi)(1-8\xi)\mathcal{D}. \tag{3.4d}$$

Especially noteworthy is that the nondimensionalized curvature ξ is positive for curvature. Thus, $\mathcal{D}$ has a singularity. Therefore, the domain of the parameters must be clarified and a special treatment is required to quantitatively describe the solution at the singular point. The family solutions in the nonlinear regime for spikes are illustrated in Figure 2.

3.3. *Singularity of the solutions for RT spikes*

Unlike the family solutions for bubbles in the nonlinear regime, the solutions for spikes exhibit singular behavior, which is also in agreement with experiments (Jacobs & Catton 1988; Meshkov & Abarzhi 2019). This singularity originates from the pole of the denominator of the velocity in Eq. (3.3), which is

$$-48\xi + A(9+64\xi^2) = 0. \tag{3.5}$$

The root of Eq. (3.3) satisfying $\xi > 0$ is $\xi_r = 3(1-\sqrt{1-A^2})/(8A)$. As the curvature reaches this singular point $\zeta_1 \to \zeta_r$, the velocity v approaches negative infinity $v \to -\infty$. Thus, the velocity at $\zeta = \zeta_r$ corresponds to the maximum velocity v_{max} for spikes $|v_{max}| = \infty$.

Due to the existence of the singularity, it is worthwhile to clarify the domain of the curvature ζ_1. To this aim, we introduce the critical curvature $\zeta_1 = \zeta_{cr}$, at which the velocity of the spike is zero $v_{cr} = 0$ with the maximum curvature $\zeta_c r = \zeta_{max}$. This definition naturally implies $\zeta_{cr} < \zeta_r < 0$. Therefore, the domain for the curvature is $\zeta_1 \in [\zeta_{cr}, \zeta_r]$ and the corresponding interval is velocity the $v \in [v_{max}, 0]$.

Nonlinear regime solutions, velocity $v/\sqrt{g(t)/k}$, shear $\Gamma/\sqrt{kg(t)}$ and curvature $|\zeta_1/\zeta_{cr}|$, for spikes are presented in Figure 2. In contrast to the solutions for bubbles, the solutions for spikes are evaluated only in the domain for the curvature is $\zeta_1 \in [\zeta_{cr}, \zeta_r]$, as previously demonstrated. Moreover, the effect of the finite-size domain kZ and the Atwood number A are compared. Bubbles in a relatively larger finite-size domain, $kZ = 5$ (black lines), have a larger velocity, a smaller shear and a small range of permissible curvature

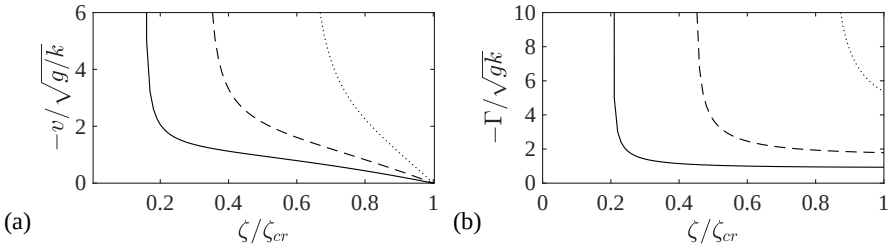

FIGURE 2. The nonlinear regime family of asymptotic solutions for spikes for the p4mm subspace group. The velocity $v/\sqrt{g/k}$, the shear $\Gamma/\sqrt{gk}$ and the curvature ξ are shown for three different Atwood numbers: $A = 0.3$ (solid lines), $A = 0.6$ (dashed lines) and $A = 0.9$ (dotted lines).

compared with bubbles in a relatively smaller finite-size domain, $kZ = 0.5$ (gray lines). As the Atwood number varies, fluids with higher contrasting densities ($A = 0.9$, solid line) have a faster velocity and a larger shear compared with fluids with similar densities ($A = 0.3$, dotted line).

Another different feature of solutions for spikes in nonlinear regimes that is different from that of bubbles is the large magnitude of the shear. Interfacial shear induces small-scale vortical structures at the vicinity of spikes and bubbles. These vortical structures are significantly pronounced near the interface of spikes (Jacobs & Catton 1988). Similar to the velocity, the shear approaches negative infinity $\Gamma \to -\infty$ as $\zeta_1 \to \zeta_r$. Therefore, the shear is maximized $\Gamma = \Gamma_{max}$ at $\zeta_1 = \zeta_r$ and the allowed interval for shear is $\Gamma \in [\Gamma_{max}, \Gamma_{cr}]$ for the domain $\zeta_1 \in [\zeta_{cr}, \zeta_r]$, where Γ_{cr} is the critical curvature.

As a conservative measure for singularity, the diagnostic parameters for spikes at $\zeta_1 = \zeta_{cr}$ are regularized by

$$\overline{v}_{max} = v_{max}\left(\frac{\zeta_1 - \zeta_{max}}{k}\right)^{1/2}, \quad \overline{\Gamma}_{max} = \Gamma_{max}\left(\frac{\zeta_1 - \zeta_{max}}{k}\right)^{1/2}. \tag{3.6}$$

The regularized solutions rescaled by Eq. (3.6) for nonlinear solutions for spikes are shown in Figure 3. For example, the velocity v is normalized by $\overline{v}_{max}$. Similarly, the curvature ζ_1 and the shear Γ are normalized by the critical curvature $\zeta_{cr} = \zeta_{max}$ and $\overline{\Gamma}_{max}$, respectively. The universality of the nonlinear solutions of spikes are observed with three different Atwood numbers, $A = 1.0, 0.5, 0.1$. The dependence between the interface dynamics, morphology and shear is shown. Moreover, the convergence behavior of Fourier amplitude is presented in Figure 3(d). We note that the convergence holds for $0 < A < 45/53 \approx 0.85$ since the solutions for the spikes in the nonlinear regime are singular and unstable.

3.4. *Special solutions*

Solutions for this family of spikes are characterized by specific conditions on the diagnostic parameters, such as the curvature ζ_1 and the velocity v. Special solutions are estabilished for the critical spike, the convergence limit spike, the Taylor spike, the Layzer-drag spike, the Atwood spike and the flat spike.

The critical spike defined above has zero velocity $v = 0$ at the critical curvature

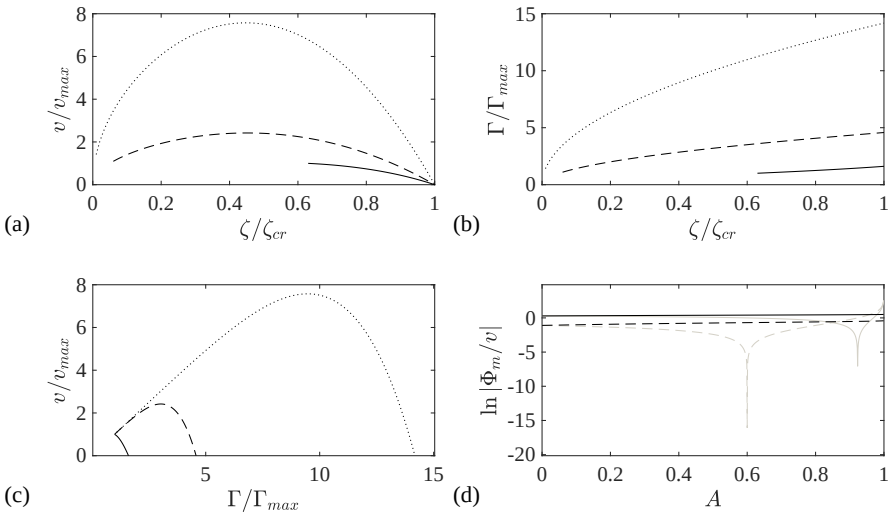

FIGURE 3. A one-parameter family of asymptotic solutions for spikes in the nonlinear regime with the subspace group p4mm. The solutions are normalized by their maximum values. The velocity $|v/v_{max}|$ and the shear $|\Gamma/\Gamma_{max}|$ as a function of the curvature $|\zeta_1/\zeta_{cr}|$ are given in (a) and (b), respectively. (c) The 1-to-1 mapping of the rescaled velocity and shear; (d) The first two Fourier amplitudes as a function of the Atwood number A. In (a,b,c), the effect of the Atwood numbers $A = 0.9$ (solid line), $A = 0.1$ (dashed line) and $A = 0.01$ (dotted line) is shown. In (d), the Fourier amplitudes for heavy fluid (black lines) and light fluid (gray lines) are plotted for the first and second harmonics as solid lines and dashed lines, respectively.

$\zeta_1 = \zeta_{cr}$. The solutions are

$$\zeta_{cr} = \frac{3}{8}k, \quad v_{cr} = 0, \quad \Gamma_{cr} = -\frac{1}{\tau}\left(\frac{t}{\tau}\right)^{\frac{a}{2}}\sqrt{\frac{6A}{1-A}}. \tag{3.7}$$

We note that the critical shear is $\Gamma_{cr} = \Gamma_{max}$. Also, the curvature and the velocity are the same as the critical solutions for the bubble.

The convergence limit spike is categorized for the spike whose Fourier amplitudes in Eq. (3.4) follow $|\Phi_1| > |\Phi_2|$ at $\zeta_1 \in (\zeta_{max}, \zeta_{cr})$ and $|\widetilde{\Phi}_1| > |\widetilde{\Phi}_2|$ at $\zeta_1 \in (\zeta_{max}, \zeta_{cn})$. Moreover, $|\Phi_1| = |\Phi_2|$ at $\zeta_1 = \zeta_{cr}$ for heavy fluid and $|\widetilde{\Phi}_1| = |\widetilde{\Phi}_2|$ at $\zeta_1 = \zeta_{cn}$ for light fluid. The solutions for the convergence limit spike at $\zeta_1 = \zeta_{cn}$ are written as

$$\zeta_{cn} = \frac{5}{24}k, \qquad v_{cn} = -\frac{1}{k\tau}\left(\frac{t}{\tau}\right)^{\frac{a}{2}}\frac{14}{3}\sqrt{\frac{10A}{3(45-53A)}},$$

$$\Gamma_{cn} = -\frac{1}{\tau}\left(\frac{t}{\tau}\right)^{\frac{a}{2}} 9\sqrt{\frac{10A}{3(45-53A)}}. \tag{3.8}$$

The curvature for the convergence limit spike has the same magnitude as that of the bubble. On the other hand, the velocity and shear approach negative infinity as $A \to 45/53 \approx 0.85$ due to the singularity. Also, we note that the velocity and the shear become zero as $A \to 0^+$. The convergence limit curvature is related to the critical curvature as $\zeta_{cn}/\zeta_{cr} = 5/9$, which implies that the convergence limit spike is less curved than the

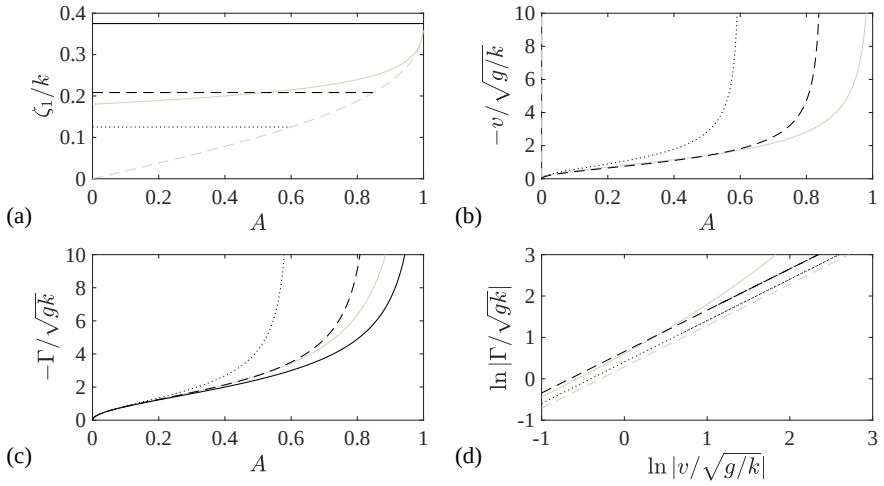

FIGURE 4. Special solutions for spikes among the one-parameter family of asymptotic solutions for p4mm. The solutions are given for the critical spike (black solid line), convergence limit spike (black dashed line), Taylor spike (black dotted line), Layzer-drag spike (gray solid line) and Atwood spike (gray dashed line).

critical spike. The Fourier amplitudes of light fluid is balanced for spike at convergence limit curvature $\zeta_1 = \zeta_{cn}$, whereas the Fourier amplitudes of heavy fluid is balanced for bubble at $\zeta_1 = \zeta_{cn}$.

The Taylor spike is a spike with a curvature $\zeta_T = 1/8k$. This definition stems from the same analogy for the Taylor bubble. The solutions for the Taylor spike at $\zeta_1 = \zeta_T$ are

$$\zeta_T = \frac{1}{8}k, \qquad v_T = -\frac{1}{k\tau}\left(\frac{t}{\tau}\right)^{\frac{a}{2}} 2\sqrt{\frac{2A}{3-5A}},$$
$$\Gamma_T = -\frac{1}{\tau}\left(\frac{t}{\tau}\right)^{\frac{a}{2}} 3\sqrt{\frac{2A}{3-5A}}. \tag{3.9}$$

We note that only at $N = 1$ for the Taylor spike, the second Fourier amplitude for light fluid is zero $\Phi_2 = 0$. The curvature for the Taylor spike is the same in magnitude as for the Taylor bubble curvature. For the Taylor spike, the velocity v_T and shear Γ_T have finite values for $0 < A < 3/5 \approx 0.6$ and approach zero as $A \to 0^+$. As $A \to 3/5 \approx 0.6$, v_T and Γ_T diverge to negative infinity. Comparisons of the Taylor spike curvature with the previous special solultions for spikes are $\zeta_T/\zeta_{cr} = 1/3$ and $\zeta_T/\zeta_{cn} = 3/5$.

The Layzer-drag spike is a spike with a velocity $v = (k\tau)^{-1}(t/\tau)^{a/2}\sqrt{2A/(1-A)}$ and has the same rationale as the Layzer-drag bubble. The solutions for the Layzer-drag spike are expressed as

$$\zeta_L = \zeta_L(k, A), \qquad v_L = -\frac{1}{k\tau}\left(\frac{t}{\tau}\right)^{\frac{a}{2}} \sqrt{\frac{2A}{1-A}},$$
$$\Gamma_L = -\frac{1}{\tau}\left(\frac{t}{\tau}\right)^{\frac{a}{2}} 12\left(9 - 64\left(\frac{\zeta_L}{k}\right)^2\right)^{-1} \sqrt{\frac{2A}{1-A}}. \tag{3.10}$$

The curvature of the Layzer-drag spike is cumbersome and is given as $\zeta_L(k, A)$. $\zeta_L =$

$\zeta_L(k, A)$ is also shown in Figure 4(a). The velocity v_L and the shear Γ_L of the solutions for the Layzer-drag spike approach zero as $A \to 0^+$. v_L and Γ_L remain finite as negative values within the range $0 < A < 1$ and become singular, diverging to negative infinity as $A \to 1^-$. The Layzer-drag solutions are further simplified at the two limits of $A \in [0, 1]$. At the limit of $A \to 1^-$, where the two fluids have very contrasting densities, the solutions for the Layzer-drag bubble are

$$\zeta_L \approx \frac{1}{8}k,\ v_L \approx -\frac{1}{k\tau}\left(\frac{t}{\tau}\right)^{\frac{a}{2}}\sqrt{\frac{2}{1-A}},$$
$$\Gamma_L \approx -\frac{1}{\tau}\left(\frac{t}{\tau}\right)^{\frac{a}{2}}\frac{1}{4}\left(\frac{3}{8}-\frac{\zeta_L}{k}\right)^{-1}\sqrt{\frac{2}{1-A}}. \tag{3.11}$$

Both v_L and Γ_L at $A \to 1^-$ become singular, with the latter being more singular than the former. At the limit of $A \to 0^+$, where the two fluids have very similar densities,

$$\zeta_L \approx \frac{1}{8}k\sqrt{9-4\sqrt{3}}, \quad v_L \approx -\frac{1}{k\tau}\left(\frac{t}{\tau}\right)^{\frac{a}{2}}\sqrt{2A},$$
$$\Gamma_L \approx -\frac{1}{\tau}\left(\frac{t}{\tau}\right)^{\frac{a}{2}}\sqrt{6A}. \tag{3.12}$$

The Layzer-drag spike is more curved for the contrasting-density fluids $A \to 1^-$ than for the similar-density fluids $A \to 0^+$. For a finite density ratio $A \in (0, 1)$, the Layzer-drag spike is related to the critical spike and Taylor spike as $\zeta_L/\zeta_{cr} \in (\sqrt{9-4\sqrt{3}}/3, 1)$ and $\zeta_L/\zeta_T \in (\sqrt{9-4\sqrt{3}}, 3)$, respectively. This ratio of curvature implies that the velocity v_L is smaller and the shear Γ_L is larger those for the Taylor bubble. The solutions in Eq. (3.10) are presented in Figure 4. Not all solutions for the Layzer-drag spike are convergent. The ratio of the curvature for the Layzer-drag spike and the convergence limit spike becomes unity $\zeta_L/\zeta_{cn} = 1$ at $A = 235/451 \approx 0.52$, and thus, the solutions for the Layzer-drag spike are not convergent beyond $A > 0.52$ (e.g., see, Figure 4(a)).

The Atwood bubble solutions are the fastest solutions among the family solutions in Eq. (3.3). These solutions are previously introduced as v_{max} for velocity and Γ_{max} for shear at $\zeta_1 = \zeta_{max}$, respectively. Thus, the curvature, the velocity and the shear follow $\zeta_A = \zeta_{max}$, $v_A = v_{max}$ and $\Gamma_A = \Gamma_{max}$, respectively. The special solutions for the Atwood spike are written as

$$\zeta_A = \kappa(A)k,\ v_A = -\frac{\phi(A)}{k\tau}\left(\frac{t}{\tau}\right)^{\frac{a}{2}}\left(\frac{k}{\zeta-\zeta_A}\right)^{\frac{1}{2}},$$
$$\Gamma_A = -\frac{\gamma(A)}{\tau}\left(\frac{t}{\tau}\right)^{\frac{a}{2}}\left(\frac{k}{\zeta-\zeta_A}\right)^{\frac{1}{2}}, \tag{3.13}$$

where

$$\kappa(A) = \frac{3(1-\sqrt{1-A^2})}{8A},\ \phi(A) = \frac{9(1-A^2)^{\frac{1}{4}}(1-\sqrt{1-A^2})^{\frac{3}{2}}}{4A^2},$$
$$\gamma(A) = \frac{3(1-\sqrt{1-A^2})^{\frac{1}{2}}}{2(1-A^2)^{\frac{1}{4}}}. \tag{3.14}$$

For the Atwood spike, the curvature ζ_A is regular whereas the velocity v_A and the shear

Γ_A are singular. The solutions in Eq. (3.14) are simplified at the two ends limit of the Atwood number A. At the limit of $A \to 1^-$, where the two fluids have very contrasting density,

$$\kappa \approx \frac{3}{8}(1-\sqrt{2(1-A)}),\ \phi \approx \frac{9}{4}\left\{2(1-A)\right\}^{\frac{1}{4}},$$
$$\gamma \approx \frac{3}{2}\left\{2(1-A)\right\}^{-\frac{1}{4}}. \tag{3.15}$$

At the limit of $A \to 0^+$, where the two fluids have very similar density,

$$\kappa \approx \frac{3}{16}A,\ \phi \approx \frac{9}{8\sqrt{2}}A,\ \gamma \approx \frac{3}{2\sqrt{2}}A. \tag{3.16}$$

The Atwood spike is less curved than the Layzer-drag spike in $A \in [0, a)$. At $A = 1$, the curvature ζ_A becomes the same curvature as the Layzer-drag curvature ζ_L and the critical curvature ζ_{cr}. the Atwood curvature increases as the Atwood number A is increased, the curvature ζ_A intersects with the curvature for the Taylor spike $\zeta_A = \zeta_T$ at $A = 3/5 \approx 0.6$ and with the curvature for convergence limit spike $\zeta_A = \zeta_{cn}$ at $A = 45/53 \approx 0.85$. $\zeta_A = \zeta_{cn}$ implies that the solutions for the Atwood spike are no longer convergent for $A > 0.85$ (e.g., see, Figure 4(a)).

Especially noteworthy is that while the curvature of both the Atwood spike and the Atwood bubble is finite, the curvature is more curved for the Atwood spike than for the Atwood bubble for fluids with highly contrasting densities whereas the opposite is true for fluids with similar densities.

A flat spike is a stagnant spike $v_f = 0$ with zero curvature $\zeta_f = 0$. The solutions for the flat spike are expressed as

$$\zeta_f = 0,\ v_f = 0,\ \Gamma_f = 0. \tag{3.17}$$

We note that while the velocity is zero for both the critical bubble and the flat bubble, the curvature, and thus the shear, is zero only for the flat bubble.

3.5. *Transition to mixing*

Classical understanding of the transition of the RT dynamics to self-similar mixing is based on a merger mechanism ascribed to the growth of horizontal scales (Alon *et al.* 1995). However, prior research on the momentum model confirms the possibility of the transition from RT dynamics to self-similar mixing given that the vertical length scale becomes the dominant scale in the system (Abarzhi 2010). Also, several experiments of RTI with high Reynolds number substantiate this occurrence of transition (Meshkov & Abarzhi 2019). Since the group theory approach in this study demonstrates the self-similar RT dynamics within the framework of the momentum model, the transition from scale-dependent dynamics to the self-similar mixing can be associated with the multiscale characteristics of nonlinear dynamics of RTI.

The transition to the self-similar mixing of spikes is addressed with the Atwood spike. The solutions for the Atwood spikes follow

$$|\zeta_A| \sim k \sim \lambda^{-1} \tag{3.18a}$$

$$|v_A| \sim \frac{1}{k\tau}\left(\frac{t}{\tau}\right)^{\frac{a}{2}}\left(\frac{k}{\zeta-\zeta_A}\right)^{\frac{1}{2}} = \left(\frac{g}{k}\right)^{\frac{1}{2}}\left(\frac{k}{\zeta-\zeta_A}\right)^{\frac{1}{2}}. \tag{3.18b}$$

Then,

$$|v| \sim \sqrt{G\lambda t^a}, \qquad |y_0| \sim t\sqrt{G\lambda t^a}. \tag{3.19}$$

The amplitude y_0 of the spikes grows as a vertical length scale comparable to the horizontal length scale λ. For $|y_0| > \lambda$, the vertical length scale becomes the dominant length scale characterizing the RTI. From the studies of the momentum model (Abarzhi 2010), the rate of loss of specific momentum (i.e., the drag force per unit mass) scales as $\sim v^2/|y_0|$. Applying the transition of the dominant length scale from λ to $|y_0|$ shows the reduction of the drag force from $\sim v^2/\lambda$ to $\sim v^2/|y_0|$. This reduced drag force leads to the acceleration of the bubble and thus provokes the transition of RTI dynamics from scale dependent to self-similar mixing. By substituting λ in Eq. (3.19) for $|y_0|$, the scalings of the velocity $|v|$ and the amplitude $|y_0|$ imply

$$|v| \sim Gt^{a+1}, \qquad |y_0| \sim Gt^{a+2}. \tag{3.20}$$

Since the spikes are singular, the growth of the amplitude z_0 can be faster than the analytic solution in Eq. (3.18). The fast growth in amplitude indicates the dominance of the vertical length scale as RTI evolves. Thus, for $|z_0| \gg \lambda$, the drag force is reduced, thus leading to self-similar mixing in Eq. (3.20). For fluids with very contrasting densities, $A \to 1^-$, the Atwood spike is highly singular and can only be self-similar.

4. Conclusions

Analytical solutions for spikes for 3D RTI under variable acceleration with a power-law time dependence are derived. The group theory is applied to describe 3D spatially periodic RT flow in the plane normal to the acceleration. The square symmetry of the flow and the effect of finite-size domains are considered for the first time. The irreducible representation of the flow potential is sought. Introducing moment expressions leads to the dynamical system for 3D RTI. Linear regime solutions follow the exponential form. Nonlinear regime solutions are derived as a continuous family of asymptotic solutions. Due to the singular behavior of the solutions for spikes, they are unstable, unlike the regular and stable solutions of bubbles. Even though the solutions exhibit singularity, the convergence of the solutions of the spikes in terms of Fourier amplitudes demonstrates that the this plausible solution for spikes in reality can move faster than the theoretically predicted value. Nonlinear regime solutions are directly related to the shear at the interface which triggers the small-scale vorticies. Also, the effect of the finite-size domain is presented. Applying fundamental scaling, special solutions of RT bubbles are identified. From the Atwood bubble invariant, multiscale character of 3D RTI is shown. Transition toward the mixing regime is addressed on the basis of scaling analysis.

REFERENCES

Abarzhi, S. I. & Inogamov, N. A. 1995 Stationary solutions in the Rayleigh-Taylor instability for spatially periodic flow. *J. Exp. Theor. Phys.* **80**, 132–143.

Abarzhi, S. I. 1996 Stationary solution of the Rayleigh-Taylor instability for spatially periodic flows: questions of uniqueness, dimensionality, and universality. *J. Exp. Theor. Phys.* **83**, 1012–1026.

Abarzhi, S. I. 2010 Review of theoretical modeling approaches of Rayleigh-Taylor instabilities and turbulent mixing. *Philos. Trans. R. Soc. A* **368**, 1809–1828.

Abarzhi, S. I. & Sreenivasan, K. R. 2010 Turbulent mixing and beyond. *Philos. Trans. R. Soc. A.* **368**, 1539–1546.

Abarzhi, S. I., Gauthier, S. & Sreenivasan, K. R. 2013 Turbulent mixing and beyond: non-equilibrium processes from atomistic to astrophysical scales. *Philos. Trans. R. Soc. A* **371**, 20120435

Alon, U., Hecht, J., Ofer, D. & Shvarts, D. 1995 Power laws and similarity of Rayleigh-Taylor and Richtmyer-Meshkov mixing fronts at all density ratios. *Phys. Rev. Lett.* **74**, 534.

Hwang, H. & Abarzhi, S. I. 2020a Two-dimensional scale-dependent Rayleigh-Taylor dynamics with variable acceleration in a finite-size domain. *Annual Research Briefs*, Center for Turbulence Research, Stanford University, pp. 371–382.

Hwang, H. & Abarzhi, S. I. 2020b Three-dimensional scale-dependent Rayleigh-Taylor dynamics with variable acceleration in a finite-size domain: Part I. Solutions of bubbles in linear and non-linear regimes. *Annual Research Briefs*, Center for Turbulence Research, Stanford University, pp. 383–395.

Jacobs, J. W. & Catton, I. 1988 Three-dimensional Rayleigh–Taylor instability Part 2. Experiment. *J. Fluid Mech.* **187**, 353–371.

Layzer, D. 1955 On the instability of superposed fluids in a gravitational field. *Astrophys. J.* **122**, 1.

Meshkov, E. E. 2013 Some peculiar features of hydrodynamic instability development. *Philos. Trans. R. Soc. A* **371**, 20120288.

Meshkov, E. E. & Abarzhi, S. I. 2019 Group theory and jelly's experiment of Rayleigh–Taylor instability and Rayleigh–Taylor interfacial mixing. *Fluid Dyn. Res.* **51**, 065502.

Mikaelian, K. O. 2014 Solution to Rayleigh–Taylor instabilities: bubbles, spikes, and their scalings. *Phys. Rev. E* **89**, 053009.